Modeling of Levitation Force for a Wireless-Moving-Levitating Light with Multiple Magnetic Fields

Guang-Zhong Cao , Jin-Chang Guo , Su-Dan Huang *, Wen-Bo Li

Shenzhen Key Laboratory of Electromagnetic Control, Shenzhen University, Shenzhen 518060, China, hsdsudan@szu.edu.cn

Abstract—This paper presents the modeling of the levitation force for a wireless-moving-levitating light (WMLL) developed in the laboratory. The mechanical structure of the WMLL is first given. A control scheme, which is used to regulate the energized current for stable, quick, and accurate levitation of the levitating disk, is then presented. Furthermore, the model of the levitation force is theoretically derived based on the Ampere' molecular current hypothesis and the Biot-Savart law. Additionally, a finite element analysis is performed to characterize the levitation force. Finally, the effectiveness of the model is verified through the experimental results.

Index Terms—Wireless-moving-levitating light, model of the levitation force, multiple magnetic fields.

I. INTRODUCTION

Wireless-moving levitating manipulation is a promising solution to fulfill certain tasks in hard-to-reach environments, such as biomanipulation, tunnel containing flammable gas, and the cleanroom for semiconductor manufacturing. This manipulation, adapting magnetic levitation technology [1], [2] and wireless power transmission (WPT) [3], [4], have the characteristics of contactless, eliminating contamination, and ecofriendly nature. The magnetic levitation technology has been successfully applied to maglev train [5], [6] and magnetic bearing [7], [8]. The WPT has been mainly used for wireless charging in consumer electronics and electric vehicles, passive radio-frequency identification (RFID), wireless actuators, etc. [9], [10] Currently, in illumination field, the rapid development of levitating lights has been shown potential application of the magnetic levitation technology and WPT. There are mainly two kinds of levitating lights have been developed. One kind of levitating light named LUNALUXX was developed by L. Verbakel I. and W. v. Eenennaam in Netherlands [11]. The other named Flyte was developed by F. Harandi and P. Mallol *et al.* in Sweden [12]. However, few literatures on the detailed study of levitating lights can be found.

A novel wireless-moving-levitating light (WMLL) with multiple magnetic fields is proposed and developed in our laboratory. Levitation force is a key factor for magnetic levitation technology of the WMLL. For the WMLL, modeling of levitation force is very important and urgently needed to solve, because it is the foundation of the design and control. Thus, this paper presents the modeling of levitation force for the WMLL.

The organization of this paper is as follows. The mechanical structure and control scheme are clarified in Section II. In Section III, the model of the levitation force of the WMLL is derived theoretically. The experiment is carried out and the experimental results are presented in Section IV. Finally, the conclusion remarks are given in Section V.

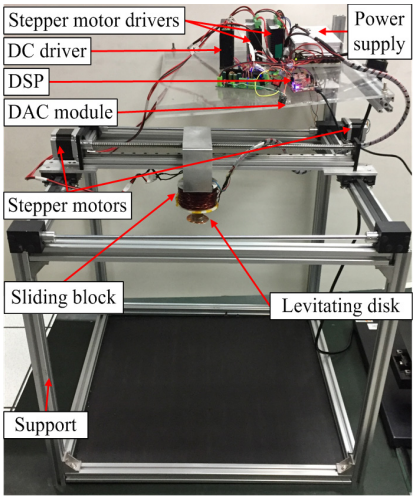

Figure 1. The oveall structure of the WMLL.

II. SYSTEM FOMULATION

A. Mechanical Strcture

The overall structure of the WMLL is shown in Fig. 1. The key components of the WMLL are two hybrid stepper motors, a sliding block, and a levitating disk. Each of the stepper motors is driven by stepper motor drivers to achieve the motion of the sliding block in each direction. The sliding block consists of an aluminum block, a coreless winding, a transmitting coil, and two linear hall-effect sensors. The cylindrical plastics is fixed on the aluminum block, and the aluminum block is assembled as moving parts. The coreless winding is wound in cylindrical plastics. The transmitting coil is mounted on the bottom of the cylindrical plastics. The two hall-effect sensors are Installed in the top and bottom of the cylindrical plastics, respectively, which are used to detect the levitating position of levitation disk. The levitating disk is composed of a receiving coil, a magnet of Neodymi-um-Iron-Boron (NdFeb), and LEDs. The levitating disk is levitated through the interaction of the NdFeb and the energized coreless winding, which moves with the motion of sliding block. The LEDs are lighted through power transferred by the transmitting and receiving coils. Other parts of the WMLL are a direct current (DC) driver, a digital signal processor

(DSP) controller, a digital-to-analogue converter (DAC), and a power supply. The DC driver is employed to energize the coreless winding. The DAC module is utilized to offer control signal to DC driver. The DSP controller implements the analog-to-digital (AD) sample, communication, calibration of the hall-effect sensors, and output of the control signal.

B. Control Scheme

Fig. 2 depicts the block diagram of the levitating position control of the levitating disk. The control signal u is approximately proportional to the amplitude of current of the coreless winding. The differential voltage of the hall-effect sensors e_h is transformed by the current of the coreless winding I based on corresponding electrical theory. Hence, there is a definite relationship between the differential voltage e_h of the hall-effect sensors and the control signal u. The differential voltage of the hall-effect sensors eh and control signal u as input, the detected levitating position z_l is calculated by a calibration method. The detected levitating position z_l is compared with the reference levitating position r, and their corresponding position error e is processed through a proportional-integral-derivative (PID) controller to generate the control signal u. The control signal u is further processed by the DC driver to generate regulated current I to energize the coreless winding. Owing to the magnetic interaction between the NdFeB and the energized coreless winding, the levitation force of the levitating disk is generated.

III. MODELING OF LEVITATION FORCE

The levitation force of the WMLL is produced by the interaction of the cylindrical NdFeB and coreless winding. Fig. 3 presents the schematic of the cylindrical NdFeB and coreless winding, and the schematic of the cylindrical NdFeB is given in Fig. 4. The model of the levitation force of the WMLL is deduced and analyzed based on finite model analysis (FEA) in this section.

As can be seen in Fig. 3 and Fig. 4, definiting that $d\boldsymbol{l}$ is a vector whose magnitude is the length of the differential element of the current loop, $P(r\cos\varphi, r\sin\varphi, h)$ is a point outside the cylindrical NdFeB and inside the coreless winding, $M(R_1\cos\theta, R_1\sin\theta, s)$ is a point in the current loop. R_1 is the radius of the NdFeB, R_2 is the inner radius of the coreless winding, and R_3 is the outer radius of the coreless winding. θ is the azimuth of M. s is the height of M. r is the radial distance of P. φ is the azimuth of P. h is the height of P. z_l is the levitating position of the NdFeB, J is the surface current density of the NdFeB. The magnetic induction $d\boldsymbol{B}$ at P generated by $I^*d\boldsymbol{l}$ is represented as

$$d\boldsymbol{B} = \frac{\mu_0}{4\pi}\cdot\frac{I^* d\boldsymbol{l}\times\boldsymbol{D}}{\boldsymbol{D}^3} \tag{1}$$

$$\boldsymbol{D} = (r\cos\varphi - R_1\cos\theta, r\sin\varphi - R_1\sin\theta, z-h) \tag{2}$$

$$d\boldsymbol{l} = R_1(-\sin\theta\boldsymbol{i} + \cos\theta\boldsymbol{j})d\theta \tag{3}$$

where μ_0 is the permeability of vacuum, $I^*=Jds$ is the current of $d\boldsymbol{l}$, and $\boldsymbol{D}$ is the vector from M to P, $\boldsymbol{i}$ and $\boldsymbol{j}$ are expressed as the unit vectors in x- and y-axes, respectively.

The magnetic induction $\boldsymbol{B}$ is detailedly deduced as

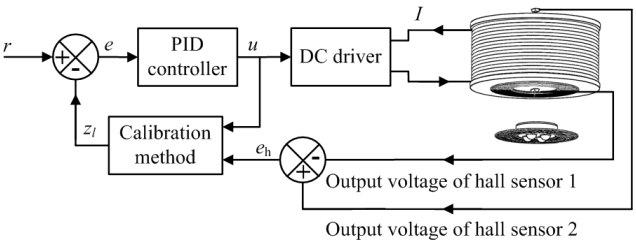

Figure 2. Block diagram of the levitating position control of the levitating disk.

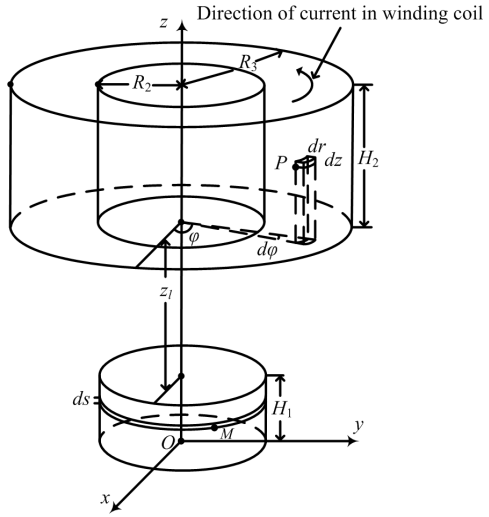

Figrue 3. Schematic of the cylindrical NdFeB and coreless winding.

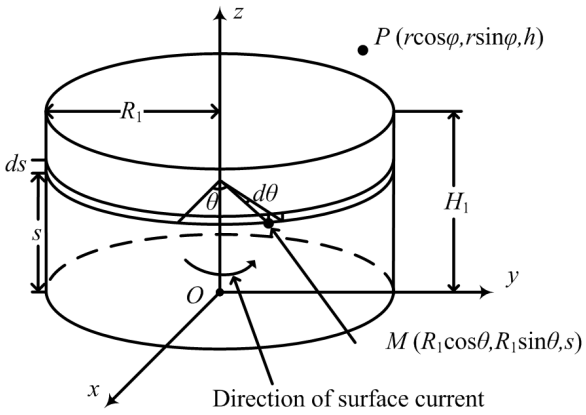

Fig 4. Schematic of the cylindrical NdFeB.

$$\begin{cases} B_x = \dfrac{\mu_0 J R_1}{4\pi}\displaystyle\int_0^{H_1}\int_0^{2\pi}\frac{(h-s)\cos\theta}{\boldsymbol{D}^3}d\theta ds \\ B_y = \dfrac{\mu_0 J R_1}{4\pi}\displaystyle\int_0^{H_1}\int_0^{2\pi}\frac{(h-s)\sin\theta}{\boldsymbol{D}^3}d\theta ds \\ B_z = \dfrac{\mu_0 J R_1}{4\pi}\displaystyle\int_0^{H_1}\int_0^{2\pi}\frac{(R_1 - r\cos(\theta-\varphi))}{\boldsymbol{D}^3}d\theta ds \end{cases} \tag{4}$$

where B_x, B_y, and B_z are the magnetic induction in x-, y-, and z-axes of $\boldsymbol{B}$, respectively.

The surface current density J is given as

$$J = \frac{2B_z}{\mu_0 R_1 \int_0^{H_1} \frac{R_1}{[R_1^2 + (H_1 - s)^2]^{\frac{3}{2}}} ds}. \quad (5)$$

Because the value B_z on the top surface of the NdFeB could be measured through the magnetometer, then the surface current density J can be calculated with the B_z according to equation (5).

Defining the differential volume of point P is

$$dv = rd\varphi dhdr. \quad (6)$$

The volume current density of the coreless winding is

$$\boldsymbol{K} = \frac{NI}{H_2 \pi (R_3^2 - R_2^2)} (-\sin\varphi \boldsymbol{i} + \cos\varphi \boldsymbol{j}) \quad (7)$$

where N is the number of turns of the coreless winding, I is the regulated current of the coreless winding.

Since the magnitude of the magnetic induction of the coreless winding is negligible compared with that of the NdFeB, the levitation force $d\boldsymbol{F}$ at P generated by the magnetic induction of the NdFeB and the coreless winding is approximately given as

$$d\boldsymbol{F} = \boldsymbol{K} \times \boldsymbol{B} dv. \quad (8)$$

Substituting (4), (6), (7) into (8), the levitation force in z-axis dF_z is derived as

$$dF_z = -cr\left[\sin\varphi \int_0^{H_1}\int_0^{2\pi} \frac{(h-s)\sin\theta}{\boldsymbol{D}^3} d\theta ds + \cos\varphi \int_0^{H_1}\int_0^{2\pi} \frac{(h-s)\cos\theta}{\boldsymbol{D}^3} d\theta ds\right] d\varphi dr dz \quad (9)$$

where

$$c = \frac{\mu_0 J R_1 NI}{4\pi^2 H_2 (R_3^2 - R_2^2)} \quad (10)$$

From equation (9), the levitation force in z-axis F_z is formulated as:

$$F_z = -c\int_{z_l+H_1}^{z_l+H_1+H_2} \int_{R_2}^{R_3}\int_0^{2\pi}\int_0^{H_1}\int_0^{2\pi} \frac{r(z-\mathrm{s})\cos(\theta-\varphi)}{\boldsymbol{D}^{\frac{3}{2}}} d\theta ds d\varphi dr dz \quad (11)$$

The levitation force is analyzed by (FEA), and the finite analysis model (FEM) of the NdFeB and the coreless winding is built. The magnetic induction distribution of the NdFeB and the magnetic induction distribution of the coreless winding whose current is less than 2 A are shown in Fig. 5 (a) and (b), respectively. The maximum amplitude of the magnetic induction of the NdFeB is 465.2% of that of the coreless winding. The result manifests that the magnetic induction produced by the NdFeB and the coreless winding can be seen as the magnetic induction distribution of the NdFeB.

The levitation force in z-axis F_z of the WMLL versus the current of coreless winding I ranging of [0, 10] A versus the levitating position z_l ranging of [0, 30] mm is manifested in Fig. 6. As can be seen from the Fig. 6, the simulation result of levitation force is consistent with that of theoretical levitation force, the levitation force in z-axis F_z ranges from 0 to 25.2 N, the levitation force in z-axis F_z changes linearly with the increase of the current of coreless winding I; On the contrary,

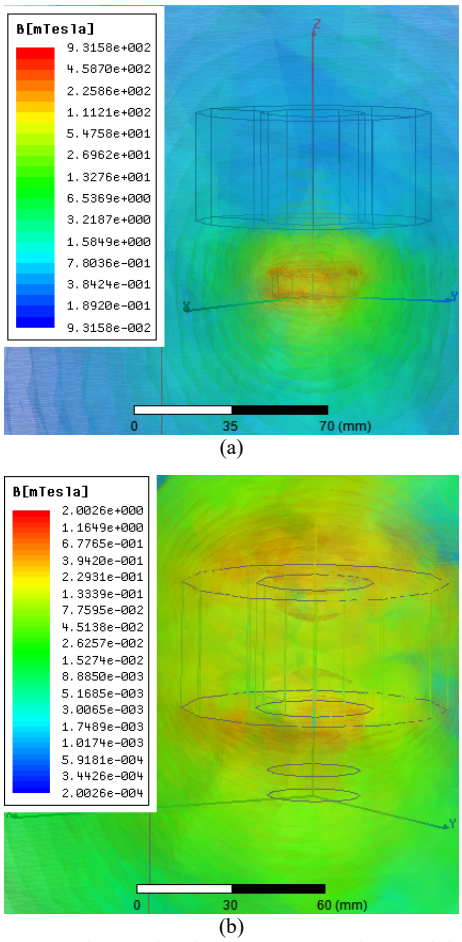

Fig 5. Magnetic induction distribution of (a) the NdFeB and (b) the coreless winding.

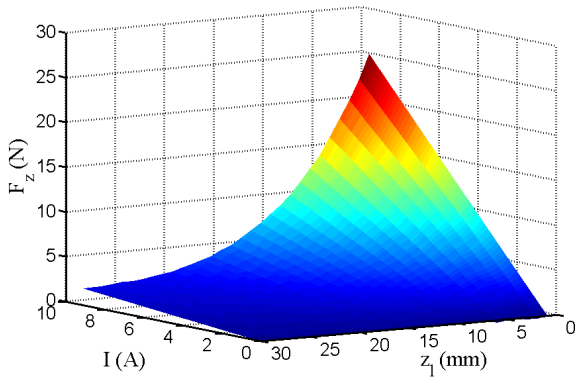

Fig 6. Levitation force in z-axis of the WMLL.

the levitation force in z-axis F_z is nonlinearly decreased with the larger levitating position z_l.

IV. Experimental Results

To further verify the effectiveness of the proposed model of the levitation force, a experimental of WMLL with stepped inputs of the desired levitating position is implemented. The experimental results of the levitating position, levitating position error, and control signal for the step input are shown in Fig. 7. From the time of 2 seconds, the levitating disk could levitate and keep in the desired position. In addition,

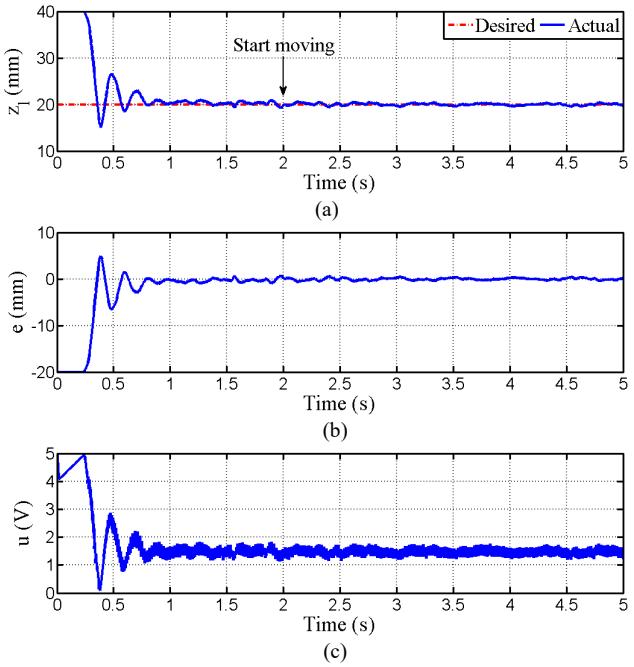

Fig. 7. Experimental results of (a) the levitating position, (b) the levitating position error, and (c) the control signal for step input.

the levitating disk follows the movement of the moving parts. The velocity of the translational motion is 5 mm/s. The steady state index is as follows: The steady-state error is within ±1.0 mm, the overshoot is 24.05%, and the settling time is 0.9 seconds at the equilibrium position of 20 mm. While the levitating disk is in a state of levitation, the control signal could accurately adjust on the basis of the real-time absolute value of the levitating position error, and the value of control signal is proportional to the levitating position error. The control signal is about 1.5 V at the equilibrium position of 20 mm for the stable levitation. The steady-state performances are approximately same with the state for without moving.

V. CONCLUSION

In this paper, the model of the levitation force of the WMLL with multiple magnetic fields was presented. The simulation of the levitation force and the experiment with a stepped inputs of the desired levitating position were implemented. The results demonstrate that the levitation forces of the theory coincide with those of the simulation; with the current range of [0, 10] A for coreless winding and the levitating position range of [0, 30] mm, the levitation force in *z*-axis varies from 0 to 25.2 N; the steady-state performances are similar for the stationary and motion of the stepper motors. The validity of the proposed model was verified. The model can provide rationale for the accurate design and control of the WMLL.

REFERENCES

[1] X. Zhang, M. Mehrtash, and M. B. Khamesee, "Dual-axial motion control of a magnetic levitation system using Hall-effect sensors," *IEEE/ASME Trans. Mech.*, vol. 21, no. 2, pp. 1129–1139, 2016.

[2] Y. Zhang, B. Xian, and S. Ma, "Continuous robust tracking control formagnetic levitation systemwith unidirectional input constraint," *IEEE Trans. Ind. Electron.*, vol. 62, no. 9, pp. 5971–5980, 2015.

[3] J. I. Agbinya, *Wireless power transfer*, 2nd ed. Danmark: River Publishers, 2015.

[4] J. Gao, G. Yan, Z. Wang, S. He, F. Xu, P. Jiang, and D. Liu, "Design and testing of a motor-based capsule robot powered by wireless power transmission," *IEEE/ASME Trans. Mech.*, vol. 21, no. 2, pp. 683–693, 2016.

[5] H.-W. Lee, K.-C. Kim, and J. Lee, "Review of maglev train technologies," *IEEE Trans. Magn.*, vol. 42, no. 7, pp. 1917–1925, 2006.

[6] S. K. Liu, B. An, S. k. Liu, and Z. J. Guo, "Characteristic research of electromagnetic force for mixing suspension electromagnet used in low-speed maglev train," *IET Electr. Power Appl.*, vol. 9, no. 3, pp. 223-228, 2015.

[7] Y. Le and K. Wang, "Design and optimization method of magnetic bearing for high-speed motor considering eddy current effects," *IEEE/ASME Trans. Mechatronics*, vol. 21, no. 4, pp. 2061–2072, 2016.

[8] J. Tang, K. Wang, and B. Xiang, "Stable control of high-speed rotor suspended by superconducting magnetic bearings and active magnetic bearings," *IEEE Trans. Ind. Electron.*, vol. 64, no. 4, pp. 3319–3328, 2017.

[9] I. Mayordomo, T. Drager, P. Spies, J. Bernhard, and A. Pflaum, "An overview of technical challenges and advances of inductive wireless power transmission," *Proceeding of the IEEE*, vol. 101, no. 6, pp. 1302–1311, 2013.

[10] J. Wu, C. Zhao, Z. Lin, J. Du, Y. Hu, and X. He, "Wireless power and data transfer via a common inductive link using frequency division multiplexing," *IEEE Trans. Ind. Electron.*, vol. 62, no. 12, pp. 7810–7820, 2015.

[11] [Online] Kickstarter PBC, https://www.kickstarter.com/projects/1185-320968/lunaluxx, 2017.

[12] [Online] Kickstarter PBC, https://www.kickstarter.com/projects/flyte/flyte- levitating-light, 2017.